Quaternary Science Reviews 344 (2024) 108945

Contents lists available at ScienceDirect

Quaternary Science Reviews

journal homepage: www.elsevier.com/locate/quascirev

Causes and consequences of natural and anthropogenically induced late Holocene hydrological variations on the largest freshwater system in the Lesser Caucasus (Lake Sevan, Armenia)

Torsten Haberzettl [a,*], Marie-Luise Adolph [a], Taron Grigoryan [b], Hayk Hovakimyan [b], Thomas Kasper [a], Norbert Nowaczyk [c], Christian Zeeden [d], Lilit Sahakyan [b]

[a] Physical Geography, Institute for Geography and Geology, University of Greifswald, Friedrich-Ludwig-Jahn-Str. 16, 17489 Greifswald, Germany
[b] National Academy of Sciences of Republic of Armenia, Institute of Geological Sciences, M. Baghramyan ave. 24a, Yerevan, 0019, Armenia
[c] Section Climate Dynamics and Landscape Evolution, GFZ German Research Centre for Geosciences, 14473 Potsdam, Germany
[d] Leibniz Institute for Applied Geophysics, Stilleweg 2, 30655 Hannover, Germany

ARTICLE INFO

Handling editor: P Rioual

Keywords:
Lacustrine sediments
Paleoclimatology
Anoxia
Hallstatt cycle
Lake level rise
Paleomagnetic secular variations

ABSTRACT

Although Lake Sevan is the largest freshwater reservoir in the Caucasus, no paleohydrological or paleoenvironmental investigations have been carried out on profundal sediments so far. Here we present high-resolution sedimentological results from a 141 cm-long sediment core covering the past $4870^{+190}/_{-245}$ cal a BP. The chronology is based on a combination of $^{137}Cs/^{210}Pb$ and radiocarbon dating supported by paleomagnetic secular variation stratigraphy, providing new inclination and declination data for the Caucasus. The time frame covered by this sequence is characterized by a long-term lake level rising trend superimposed by smaller-scale hydrological variations which is in agreement with the rest of the Lake Sevan basin. In the presented sedimentary sequence, the superimposed hydrological variations seem to be coherent with the Hallstatt and Eddy cycles.

A distinct shift towards wetter conditions is observed between 2500 and 2000 cal a BP resulting in a very high lake level. An artificial lake level drop of about 20 m in the 20th century led to anoxic conditions similar to the ones during a low lake level at $4870^{+190}/_{-245}$ cal a BP. This study shows that under natural conditions Lake Sevan was able to recover from this oxygen deficit when the lake level increased, implying that this would also happen to the artificially lowered lake today if the lake level were raised.

1. Introduction

Large lakes in high mountainous areas are the basis of life for the local population (Vardanyan et al., 2018). They are important ecosystems providing invaluable ecosystem services (Mischke, 2020) and economic resources (e.g., fishery or tourism). Therefore, such lakes are vital for the stable economic development of these regions (Vardanyan et al., 2018). Although Lake Sevan, as one of the largest freshwater reservoirs in Eurasia, is considered a natural and cultural treasure and of major importance for the population of Armenia (Gevorgyan et al., 2022), it is also an example for severe ecosystem degradation caused by anthropogenic impact. Suffering from excessive nutrient input, biodiversity loss, overfishing, water abstraction, and habitat degradation, it is one of the most degraded freshwater ecosystems worldwide (Gabrielyan et al., 2022). Consequently, the recovery of natural environmental conditions is a top environmental priority of the Republic of Armenia (Jenderedjian et al., 2012).

Currently situated at an elevation of 1900.4 m asl (Avagyan et al., 2023), Lake Sevan experienced drastic lake level changes during the recent past: In ~50 years, the lake level has decreased artificially by > 19 m due to water abstraction but ecological consequences were not considered (Gabrielyan et al., 2022). Before the lake level lowering during the early 20th century, the lake level showed great oscillations of 90 cm in 1906 CE (Loewinson-Lessing, 1929). In 1927 CE it was between 1915.54 (Gabrielyan et al., 2022) and 1916.20 m asl (Wilkinson, 2020) with annual lake level variations of 42–60 cm. At that time Lake Sevan was oligotrophic in its natural regime and water loss occurred predominantly by evaporation (Wilkinson, 2020). The depth during the early 20th century proved to be sufficient to form a thick hypolimnion during summer with an oxygen content of 8 mg l^{-1} (>80% saturation)

* Corresponding author.
E-mail address: torsten.haberzettl@uni-greifswald.de (T. Haberzettl).

https://doi.org/10.1016/j.quascirev.2024.108945
Received 4 July 2024; Received in revised form 29 August 2024; Accepted 3 September 2024
Available online 18 September 2024
0277-3791/© 2024 The Authors. Published by Elsevier Ltd. This is an open access article under the CC BY license (http://creativecommons.org/licenses/by/4.0/).

(Legovich et al., 1973).

In 1933 CE, the outflow, River Hrazdan, was dredged and a tunnel below the lake surface, which opened in 1949 CE, was constructed to provide more water from Lake Sevan for hydroelectric power and irrigation. As a result, the water level dropped by ~1 m per year in the 1950s (Hovanesian and Bronozian, 1994; Jenderedjian et al., 2012; Wilkinson, 2020) i.e., 13.7 m by 1959 CE (Gulakyan and Wilkinson, 2002). During the 1960s, the water level stabilized at ~18 m below the early 20th century water level but continued to fall reaching its lowest level at 1896.32 m asl resulting in a water level almost 20 m below the one of the early 20th century (Gabrielyan et al., 2022). To counteract the low lake level, the Arpa-Voratan extension of the Arpa-Sevan Tunnel was built to transfer water from other catchments into Lake Sevan. In the following, the lake level started to increase again in 2003 CE and by 2014 CE the water level had risen by 3.84 m from 1896.32 to 1900.16 m asl or 1900.12 m asl in 2015 CE (Wilkinson, 2020). Since 2013 the water level has remained relatively stable with annual fluctuations of about only 5–30 cm (Gabrielyan et al., 2022).

The lake level decrease resulted in the destabilization of all hydroecological processes and has changed the system from being oligotrophic to eutrophic (Ulyanova, 1993; Hovanesian and Bronozian, 1994; Gulakyan and Wilkinson, 2002) causing anoxic bottom-water conditions. However, increased anoxic conditions are not only related to eutrophication. The main responsible factor is the reduction of the hypolimnion and its oxygen reserve (Legovich et al., 1973). The volume of the hypolimnion of Small Sevan (northwestern basin, Fig. 1) decreased by five times and completely disappeared in Big Sevan (southeastern basin, Fig. 1) (Hovanesian and Bronozian, 1994). This resulted in seasonally anoxic conditions (1–4 months) near the bottom of the profundal zone (Hovanesian and Bronozian, 1994; Jenderedjian et al., 2012; Wilkinson, 2020) of Small Sevan, while sediments in the shallow parts are predominantly oxidized. As depth increases, the silt therefore becomes darker and finally black. During the stagnation period (fall), silts are covered by a white layer of precipitated chalk (Jenderedjian et al., 2012) because $CaCO_3$ precipitation increased with the shift from oligotrophic to mesotrophic conditions (Ulyanova, 1993). In Lake Sevan, several factors contribute to an increase in $CaCO_3$ precipitation with a lake level lowering: (I) a change in the morphometry of the lake warms up deeper water masses, (II) increased productivity, especially blue-green algae, promotes a reduction of CO_2 and phosphorous, and (III) an increased number of particles in the water including terrigenous contributions act as mass centers for crystallization (Ulyanova, 1993).

The climatic history of the entire Lesser Caucasus on longer time scales is still poorly understood (Sherriff et al., 2019) and only few studies investigated the Holocene history of Lake Sevan concluding that the water level varied considerably (Wilkinson, 2020): Indirect information for the Late Holocene development of Lake Sevan exists from the Vanevan peat bog (Robles et al., 2022) and the Tsovinar-1 peat section (Hayrapetyan et al., 2023) which are located close to the southern shore of Lake Sevan (Fig. 1). More direct information is available from outcrops and archaeological sites exposed after the modern anthropogenic lake level lowering at Norashen and Lchashen (Aslanian, 1984) as well as from the Artanish peninsula (Avagyan et al., 2023; Hovhannisyan et al., 2023) (Fig. 1).

The question of when Lake Sevan developed into the lake system known before the artificial lowering is still debated. While there is a consensus that it developed by a damming of the outflow Hrazdan River by lava flows (Aslanian, 1984; Avagyan et al., 2020), the timing is less clear. Some place this development simply to the Holocene (Avagyan et al., 2020) whereas others date it somewhat more precisely to the Early Holocene (Gorbatov et al., 2019), between 900 and 800 BCE (Hovhannisyan et al., 2023) or to 2000 a BP (Wilkinson, 2020). Nevertheless, lacustrine sediments of Holocene age at 1934 m asl at site Sevan 1 (Fig. 1) suggest a lake level at least 18 m above the level before the artificial lowering at some point during the Holocene (Sherriff et al., 2019).

Up to now, only limited information exists about more distal profundal sediments from Lake Sevan providing continuous information. In Big Sevan, 3–4.5 m-long undated vibra cores were retrieved along four profiles in 1960 CE (Sarkisyan, 1962); three were close to the shoreline and only one was oriented NNE-SSW across Big Sevan (Satian and Chilingaryan, 1994). In Small Sevan, it appeared impossible to recover cores or collect samples below 20 m water depth (Karakhanyan et al., 2017). Most studies, that have been carried out so far, focused on micropaleontological investigations such as ostracods (Wilkinson et al., 2005; Wilkinson and Gulakyan, 2010) or volcanic ahes (Satian et al., 1968). Chemical investigations, let alone multi-proxy approaches, have rarely been done, although already at the end of the last millennium, it became clear that the Holocene history of Lake Sevan is of great interest (Aslanian, 1984) and there is a great need to study the present-day

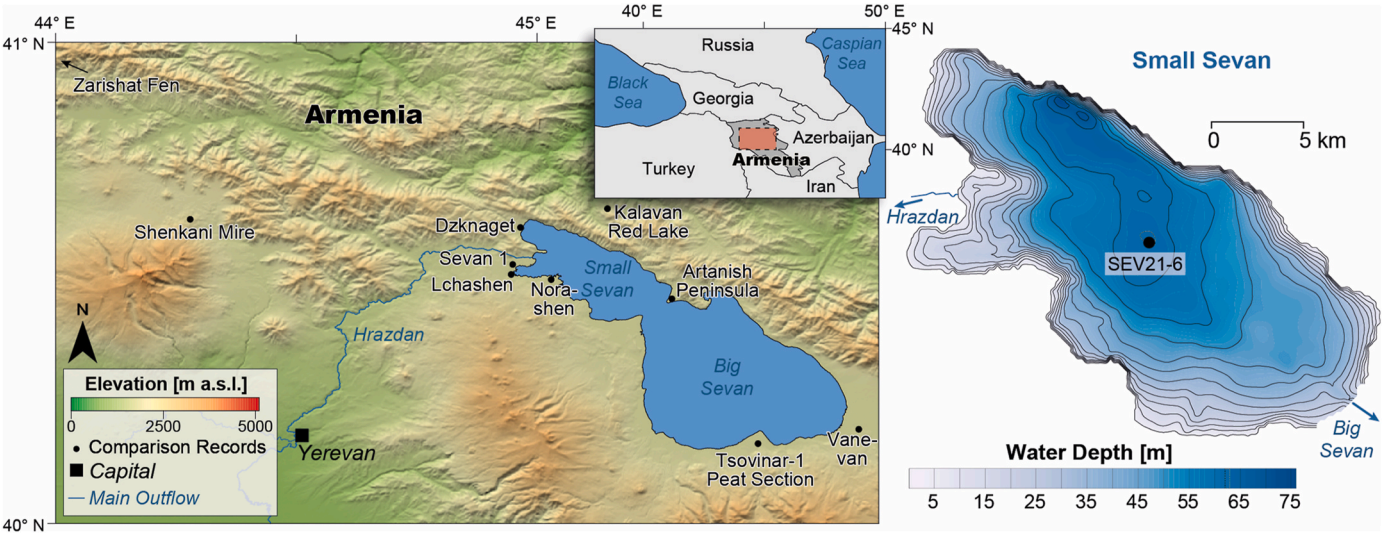

Fig. 1. Left: Location of Armenia within the Caucasus region (inset). Map of the research area showing locations mentioned in the text: Vanevan (Robles et al., 2022), Tsovinar-1 Peat Section (Hayrapetyan et al., 2023), Artanish Peninsula (Hovhannisyan et al., 2023), Kalavan Red Lake (Joannin et al., 2022), Lchashen (Aslanian, 1984), Sevan 1 (Sherriff et al., 2019), Dzknaget (Sayadyan et al., 1974; Aslanian, 1984; Vardanyan et al., 2018; Gorbatov et al., 2019), Shenkani Mire (Cromartie et al., 2020), Zarishat Fen (Joannin et al., 2014). Underlying base map: Digital Elevation Model based on CGIAR-CSI SRTM (Jarvis et al., 2008). Right: Bathymetry of Small Sevan based on Shikhani et al. (2021). SEV21-6 was recovered from the central basin at a water depth of 65 m.

conditions of sediment accumulation in lakes in order to understand their history and to determine their future status (Alekin and Ulyanova, 1994). To understand the history of Lake Sevan, causes for changes and their consequences are crucial to accurately predict its future state (Hayrapetyan et al., 2023).

Here we present sedimentological data from gravity cores from the distal profundal zone of Lake Sevan, which has never been accessed for paleoenvironmental reconstructions. Subsequently, we will set this data in context with existing investigations around this important ecosystem.

2. Site description

Lake Sevan is located in the Gegharkunik Province, 60 km to the north of the capital of Armenia, Yerevan (Fig. 1). With a length of ~70 km, a width of ~50 km at an elevation of 1900 m asl, it is one of the largest freshwater high-mountain lakes, surrounded by peaks rising to 3598 m asl (Wilkinson, 2020). The W, SW, and S of Lake Sevan are dominated by the Gegham and Vardenis volcanic highlands while the north-eastern shore of the lake is an ophiolitic structure (Karakhanyan et al., 2017; Avagyan et al., 2020).

The lake itself is structured in two parts: the larger southern part called Big Sevan has a maximum water depth of 35 m whereas the northern smaller part called Small Sevan has a water depth of 65 m in the center and a maximum water depth of 83 m close to the northern shore (Fig. 1) as a result of active tectonics. Lake Sevan has 28 inflowing rivers (four into Small and 24 into Big Sevan) and is also fed by two large springs but has only one outflow in the northern part of the lake called the Hrazdan River (Gulakyan and Wilkinson, 2002; Avagyan et al., 2020; Wilkinson, 2020).

Lake Sevan's and Armenia's climate in general is dominated by dry and cold air masses from the Siberian High in winter. If these air masses are weak, they are replaced by the Westerlies associated with the North Atlantic Oscillation. In summer, a warm and dry climate is related to the Arabian subtropical high pressure in the west and the Asian depression in the east (Joannin et al., 2014; Robles et al., 2022). The lake experiences an annual precipitation of 400–800 mm (Acopian Center for the Environment, 2018), a negative water balance with an evaporation of 800 mm a^{-1}, and a turnover rate of 50 years (Leroyer et al., 2016; Robles et al., 2022).

3. Materials and methods

To explore the potential of sediments from Lake Sevan, 16 gravity cores (51–141 cm length) were recovered from both parts of the lake in October 2021 using a 63 mm diameter UWITEC gravity coring system with a hammering device (www.unitec.at). Sediment cores were transported to the Physical Geography department of the University of Greifswald where they were stored in dark and cool conditions at 4 °C until further processing. Due to its length of 141 cm, for transport sediment core SEV21-6 had to be split into two sections at 42 cm sediment depth. In the laboratory, sediment cores were cut lengthwise using a modified manual core splitter (Ohlendorf et al., 2011) and processed according to standard protocols of the laboratory of the Physical Geography department of the University of Greifswald. This includes separation of the two core halves with two sharpened blades, digital imaging, lithological descriptions and measurements of magnetic susceptibility using a Bartington MS2E point sensor in 5 mm resolution. XRF-scanning was carried out in a 2-mm resolution at GEOPOLAR (Geomorphology and Polar Research), University of Bremen, first with a Cr-tube and later with a Mo-tube using an ITRAX system. Subsequently, results from the individual elements with >100 pa were compared between the two datasets (Cr and Mo), and only the dataset yielding higher values was considered for center-log ratio transformation which was carried out separately for the Cr and Mo datasets. Correlations within the Cr and Mo datasets were calculated using Excel. Fe/Mn-ratios were calculated using non-transformed Mo data.

Destructive analyses focused on sediment core SEV21-6 (40.53016°N, 45.12067°E, Fig. 1) from the central part of Small Sevan. To remove carbonates and organic material for grain size analyses, subsamples were treated with 2 ml hydrochloric acid (HCl, 10%) and 5 ml hydrogen peroxide (H_2O_2, 10%). Residues were dispersed overnight with 5 ml tetrasodium pyrophosphate ($Na_4P_2O_7$ * 10 H_2O, 0.1 M) in an overhead shaker. Subsequently, samples were measured in several runs using a Laser Diffraction Particle Size Analyzer (Fritsch Analysette 22) until a reproducible signal was obtained. The first reproducible run was used to calculate grain-size statistics using GRADISTAT 9.1 (Blott and Pye, 2001).

For Total Inorganic Carbon (TIC) determination in a 1-cm resolution, subsamples were freeze-dried. Prior to measuring Total Carbon (TC) using a CNS elemental analyzer (EuroEA, Eurovector), dried samples were ground in a mortar and homogenized. For determination of Total Organic Carbon (TOC), subsamples were treated with 3 and 20% HCl at 80 °C to remove any carbonates and then measured with the same device again. TIC was calculated as the difference between TC and TOC.

Dating by ^{210}Pb and ^{137}Cs was carried out on parallel sediment core SEV21-5 (Table 1). Sub-samples were analyzed for ^{210}Pb, ^{226}Ra, and ^{137}Cs by direct gamma assay in the Liverpool University Environmental Radioactivity Laboratory, using Ortec HPGe GWL series well-type coaxial low background intrinsic germanium detectors (Appleby et al., 1986). ^{210}Pb was determined via its gamma emissions at 46.5 keV, and ^{226}Ra by the 295 keV and 352 keV γ-rays emitted by its daughter radionuclide ^{214}Pb following three weeks of storage in sealed containers to allow radioactive equilibration. ^{137}Cs was measured by its emissions at 662 keV. The absolute efficiencies of the detectors were determined using calibrated sources and sediment samples of known activity. Corrections were made for the effect of self-absorption of low energy γ-rays within the sample (Appleby et al., 1992). Supported ^{210}Pb activity was assumed to be equal to the measured ^{226}Ra activity, and unsupported ^{210}Pb activity was calculated by subtracting supported ^{210}Pb from the measured total ^{210}Pb activity. Ages were then transferred to sediment core SEV21-6 using lithological marker layers and magnetic susceptibility.

For radiocarbon dating, bulk samples from sediment core SEV21-6 were sent to Beta Analytic (Table 2). Age-depth modelling was carried out with the R software package 'rbacon' (Blaauw and Christen, 2011) using the IntCal20 calibration data set for radiocarbon ages (Reimer et al., 2020). In the following, ages are reported as 'rbacon'-derived mean ages and the uncertainty is based on the upper and lower limits of the 95 % confidence interval. Radiocarbon ages published in earlier works were recalibrated with the same calibration data set in the online version of the Calib 8.2 software (Stuiver et al., 2020). In the following conventional radiocarbon ages will be labeled as 'a BP' whereas calibrated radiocarbon ages will be labeled 'cal a BP'. To check the quality of the chronology, a u-channel was extracted from SEV21-6 and transported to the GFZ German Research Centre for Geoscience, Potsdam. To measure natural remanent magnetization (NRM) a cryogenic 2G Enterprises 755 SRM long-core magnetometer was used. The NRM was alternating field (AF) demagnetized in steps of 0, 5, 10, 15, 20, 30, 40, 50, 65, 80, and 100 mT. Inclination and declination were calculated using the characteristic remanent magnetization (ChRM) determined by principal component analysis (PCA) (Kirschvink, 1980) executed in an in-house GFZ software. The median destructive field (MDF) and maximum angular deviation (MAD) values were calculated with the same software package. To take the edge effect into account, the uppermost and lowermost 5 cm of each data set were plotted in grey also accounting for the edge effect between the two sections of SEV21-6. For the same reason, the age at the top of plots begins at 0 cal a BP (1950 CE). Declination data are relative and centered to zero since the azimuth could not be controlled during coring.

Time series analysis was carried out in the R computation environment using the 'astrochron' package (Meyers, 2014; R Core Team, 2024). A Taner filter (Taner, 1992) was used for extracting frequency

Table 1
Fallout radionuclide concentrations and ^{210}Pb chronology of Lake Sevan sediment core SEV21-5.

Sediment Depth (cm)	Total ^{210}Pb (Bq kg^{-1})	Error (± Bq kg^{-1})	Unsupported ^{210}Pb (Bq kg^{-1})	Error (± Bq kg^{-1})	Supported ^{210}Pb (Bq kg^{-1})	Error (± Bq kg^{-1})	^{137}Cs (Bq kg^{-1})	Error (± Bq kg^{-1})	Dry Density (g cm^{-2})	Age (year CE)	Error (a)
0.5	441.2	24.7	424.3	25.0	16.9	4.5	24.7	3.3	0.0	2021	0
2.5	501.7	19.4	483.5	19.6	18.2	3.4	60.2	3.1	0.12	2019	1
4.5	228.0	17.2	207.6	17.6	20.4	3.9	73.6	3.6	0.53	2011	2
6.5	210.7	14.0	188.2	14.3	22.5	2.7	82.4	3.3	1.03	2003	2
7.5	169.6	13.5	148.3	13.9	21.3	3.4	96.1	3.4	1.53	1996	2
8.5	146.0	15.1	125.4	15.4	20.6	3.3	157.2	4.2	1.79	1992	2
9.5	126.1	12.2	104.2	12.5	21.8	2.6	139.6	3.6	2.06	1989	2
10.5	126.2	10.7	104.9	10.9	21.3	2.2	134.4	3.4	2.34	1986	3
12.5	116.9	10.0	96.3	10.2	20.6	2.0	60.7	2.3	2.63	1983	3
14.5	106.9	13.8	89.4	14.4	17.5	4.1	64.1	3.5	3.15	1978	3
16.5	93.8	12.9	74.0	13.3	19.8	3.4	76.9	3.1	3.61	1973	3
18.5	119.7	12.4	97.9	12.8	21.8	3.3	91.7	3.2	4.04	1969	3
20.5	111.9	13.2	86.1	13.6	25.8	3.4	16.1	2.4	4.47	1963	4
22.5	84.2	10.2	56.9	10.5	27.3	2.8	7.4	1.6	4.88	1956	5
24.5	37.6	17.6	9.7	18.2	27.9	4.7	2.7	2.6	5.31	1949	7
26.5	20.6	13.6	−3.5	13.9	24.1	2.9	0.0	0.0			
28.5	23.3	9.6	1.9	9.8	21.4	2.1	2.7	1.7			
30.5	22.8	11.4	2.9	11.8	19.9	3.1	0.0	0.0			
32.5	20.7	11.6	0.7	12.1	20.0	3.2	2.8	2.0			
35.5	28.4	11.3	8.7	11.7	19.7	3.1	0.0	0.0			

Table 2
Radiocarbon age determinations on sediment core SEV21-6.

Sediment Depth (cm)	Conventional Radiocarbon Age (a BP)	Error (a)	δ13C (‰)	Material	Laboratory Number
0	1410	30	-29.7	Bulk Organic Matter	Beta - 611062
47	1380	30	-26.1	Bulk Organic Matter	Beta - 611064
97	3350	30	NA	Bulk Organic Matter	Beta - 611063
139	4280	30	-25.3	Bulk Organic Matter	Beta - 611065

components from time series.

4. Results and interpretation

4.1. Lithology

The 141 cm-long sediment record SEV21-6 from the deepest part of Small Sevan can be divided in five lithological units (Fig. 2). Unit A (141-125 cm) consists of thick alternating white and brown laminae in mm-scale. Unit B (125-97 cm) is similar to unit A but laminae are thinner in a sub-millimetric-scale. Above sediments consist of several cm-thick rather homogenous brownish sections which are lighter in unit C (97-75 cm) and darker in unit D (75-13 cm) before thick white layers in cm-scale followed by a distinctly thinner lamination occur at the core top in Unit E (13-0 cm, Fig. 2).

4.2. Chronology

4.2.1. ^{137}Cs/^{210}Pb ages

Total ^{210}Pb activity (Fig. 3) reached equilibrium with the supporting ^{226}Ra at a sediment depth of ~25 cm (Table 1). Unsupported ^{210}Pb declined irregularly with depth and concentrations fell steeply in the uppermost 9 cm of the core but then remained relatively constant down to a sediment depth of ~20 cm. Below 20 cm, a very abrupt decline to values close to the limit of detection in the 24–25 cm sample suggests a hiatus in the sediment record at around this depth.

The ^{137}Cs record has two distinct peaks (Fig. 3). The more recent, between 8 and 11 cm, most probably records fallout from the 1986 CE Chernobyl accident. The earlier feature, between 17 and 20 cm, may record the early 1960s fallout maximum from the atmospheric testing on nuclear weapons. Traces of ^{241}Am, also a product of nuclear weapons fallout (Appleby et al., 1991), were observed in the 18–19 cm sample.

Dates calculated using the CRS ^{210}Pb dating model (Appleby and Oldfield, 1978) place 1986 within the 8–9 cm slice, which is in good agreement with the 1986 CE ^{137}Cs date. However, 1963 CE is placed within the 14–15 cm slice, significantly higher than the corresponding depth suggested by the ^{137}Cs record. The discrepancy might be due to loss of a significant part of the ^{210}Pb inventory caused by the potential hiatus in the record below 20 cm. Corrected ^{210}Pb dates have been calculated by applying the CRS in a piecewise way using the ^{137}Cs dates as reference points (Appleby, 2001).

4.2.2. Radiocarbon ages

A radiocarbon age of 1410 ± 30 a BP at the sediment surface (Table 2) indicates that either strong reworking occurs today or that Lake Sevan suffers from a hard water effect. We attribute the age offset at the surface to reworking of older sediments resulting from the lake level low stand in recent years, because i) the age of 1380 ± 30 a BP at 47 cm is younger than the overlying age and ii) the sedimentation rate is rather constant in the lower part of the record despite distinct variations in the lithology, approximately tying ^{210}Pb ages if a straight line is drawn through the three remaining radiocarbon ages (Fig. 3). This is in accordance with observations that material, which was previously deposited subaquatically, is readily eroded today. In addition to that, radiometric ages of wood (1010 ± 250 a BP) and shells of mollusks (940 ± 220 a BP), which were sampled in a 10 cm sediment interval in an outcrop at the so-called Dzknaget I section (western part of Lake Sevan, Fig. 1) (Aslanian, 1984), match very well also pointing to the absence of a reservoir effect. Therefore, a hardwater effect seems to be negligible, although major parts of the catchment consist of carbonate rocks. However, limestones at the north-eastern shore are fissureless and impermeable and runoff after rain or snowmelt forms small intermittent streams that instantly drain the area instead of weathering the limestone in underground reservoirs (Ginsberg, 1929). A somewhat higher capacity for storing water is found in limestones on the north-western shore of Lake Sevan with well-expressed latitudinal fissures, but due to their slight thickness, the outflow of water is negligible (Turtsev,

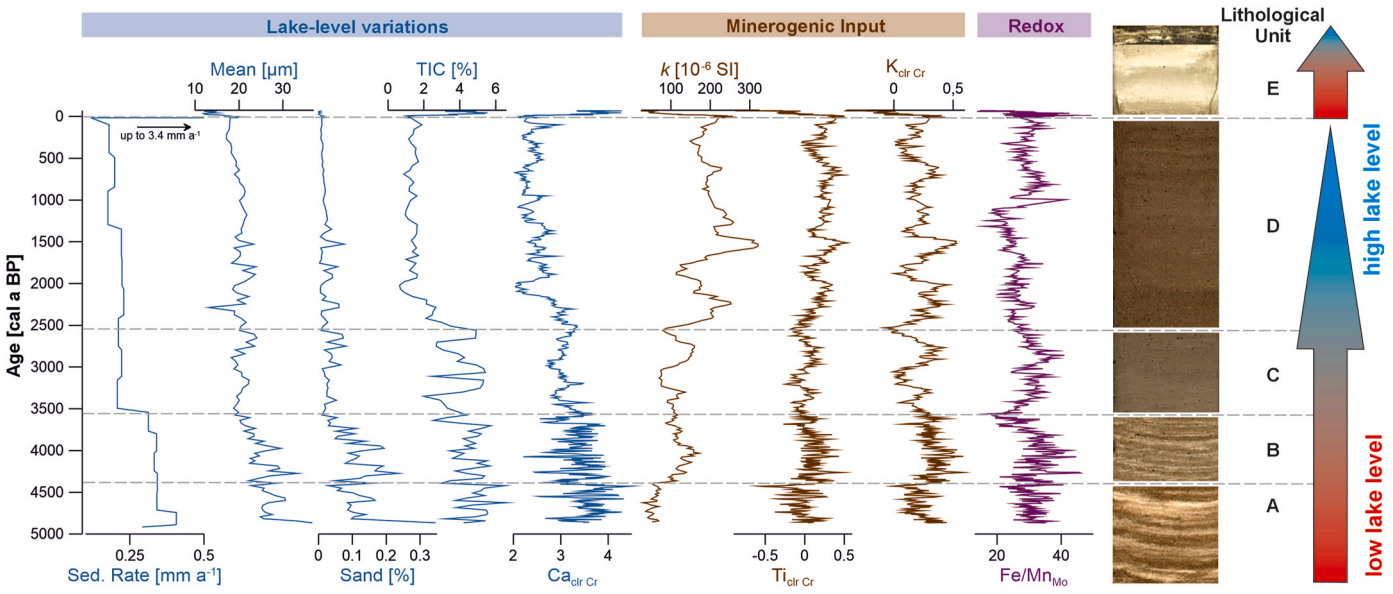

Fig. 2. Lake-level variation indicators (sedimentation rate, grain size mean, sand content, Total Inorganic Carbon (TIC), center-log-ratio transformed XRF-scanning based Calcium ($Ca_{clr\ Cr}$) measured with a Cr-tube), followed by minerogenic input parameters (magnetic susceptibility (*k*) and center-log-ratio transformed XRF-scanning based titanium and potassium ($Ti_{clr\ Cr}$ and $K_{clr\ Cr}$) measured with a Cr-tube) and redox indicator XRF-scanning based iron-manganese-ratio (Fe/Mn_{Mo}), for which the individual elements were measured with a Mo-tube, plotted next to representative images of the lithological units (for better visibility representative images of units A and E are enlarged to the top and to the bottom. Arrows at the right indicate periods of lake level rises.

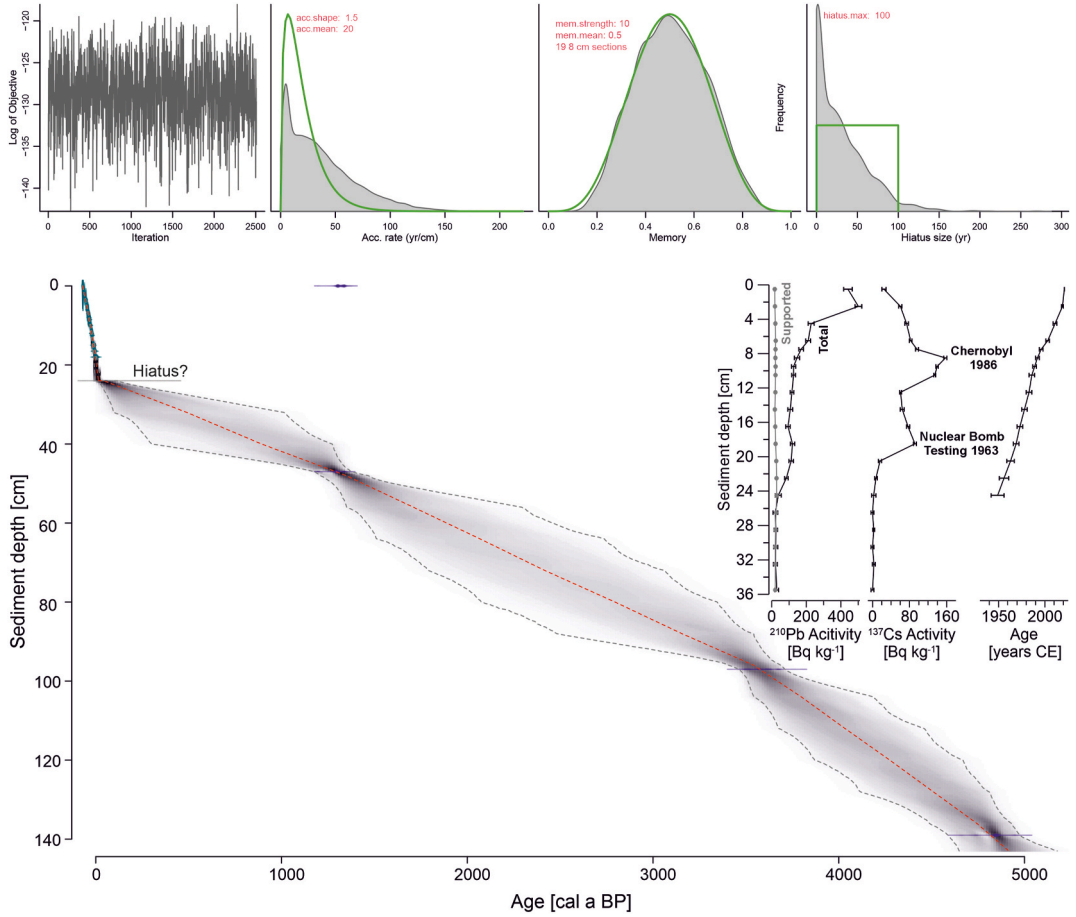

Fig. 3. Chronology for sediment core SEV21-6 from Lake Sevan based on $^{137}Cs/^{210}Pb$ and radiocarbon ages. The top left panel shows the Markov Chain Monte Carlo iterations, followed by prior (lines) and posterior densities (area fills) for mean accumulation rate, memory and hiatus size. Mean ages (red line) and 95 % confidence intervals (grey areas) are shown in the lower panel. The location of a potential hiatus of short duration is indicated by a line. Inset: $^{210}Pb/^{137}Cs$ results show a distinct peak for the Chernobyl accident of 1986 CE as well as the nuclear bomb testing in 1963 CE.

1929). Although the surface of the northern shore is composed of weathered limestones, water descending the slope begins to be raised to surface by capillary action and subsequently evaporates (Zavalishin, 1929). Consequently, measured values of the water hardness of springs were 0.9, 1.9, 2.1 and 5.4 °dH at the western shore (Kazakov, 1929) and 0.8–2.0 °dH at the north-western shore (Turtsev, 1929).

4.2.3. *Paleomagnetic secular variations and chronology*

Additional support for the presented chronology comes from paleomagnetic analyses. NRM intensities range from 0.7 to 33.1 mA m^{-1} and MDF values from 11.4 to 40.5 mT. ChRM inclination and declination show distinct changes (Fig. 4). Inclination ranges from 54 to 77°N and intersects the one expected, based on a geocentric axial dipole model (GAD = 59.68°), several times. Declination stretches over 47°, which in general is typical for paleomagnetic secular variations (Haberzettl et al. 2015, 2021). Well-preserved and stable single-component magnetization is indicated by low MAD values (Stoner and St-Onge, 2007) that are generally below 4.3°, except for the uppermost 7 cm of the record (Fig. 4).

Although being located at a great distance, inclination and declination data from Lakes Issyk-Kul (Gómez-Paccard et al., 2012) and Baikal (Peck et al., 1996) show similar patterns (Fig. 4), supporting the dating approach for SEV21-6. Surprisingly paleomagnetic variations measured in a closer distance but only to the (south-)west of Lake Sevan show almost no similarities at all and hence have not been plotted in this comparison. This discrepancy might be caused by an influence of the Levantine Iron Age geomagnetic Anomaly (LIAA), which spanned the first half of the first millennium BCE and is not yet well understood (Rivero-Montero et al., 2021) especially as far as the geographical extent is concerned (Ertepinar et al., 2020). Analyses suggest that the source of the LIAA is located in the Levantine region vanishing to the north, west and east (Rivero-Montero et al., 2021). In addition to this, predictions of global geomagnetic field models are dominated by these records to the (south-)west and have therefore also not been considered for

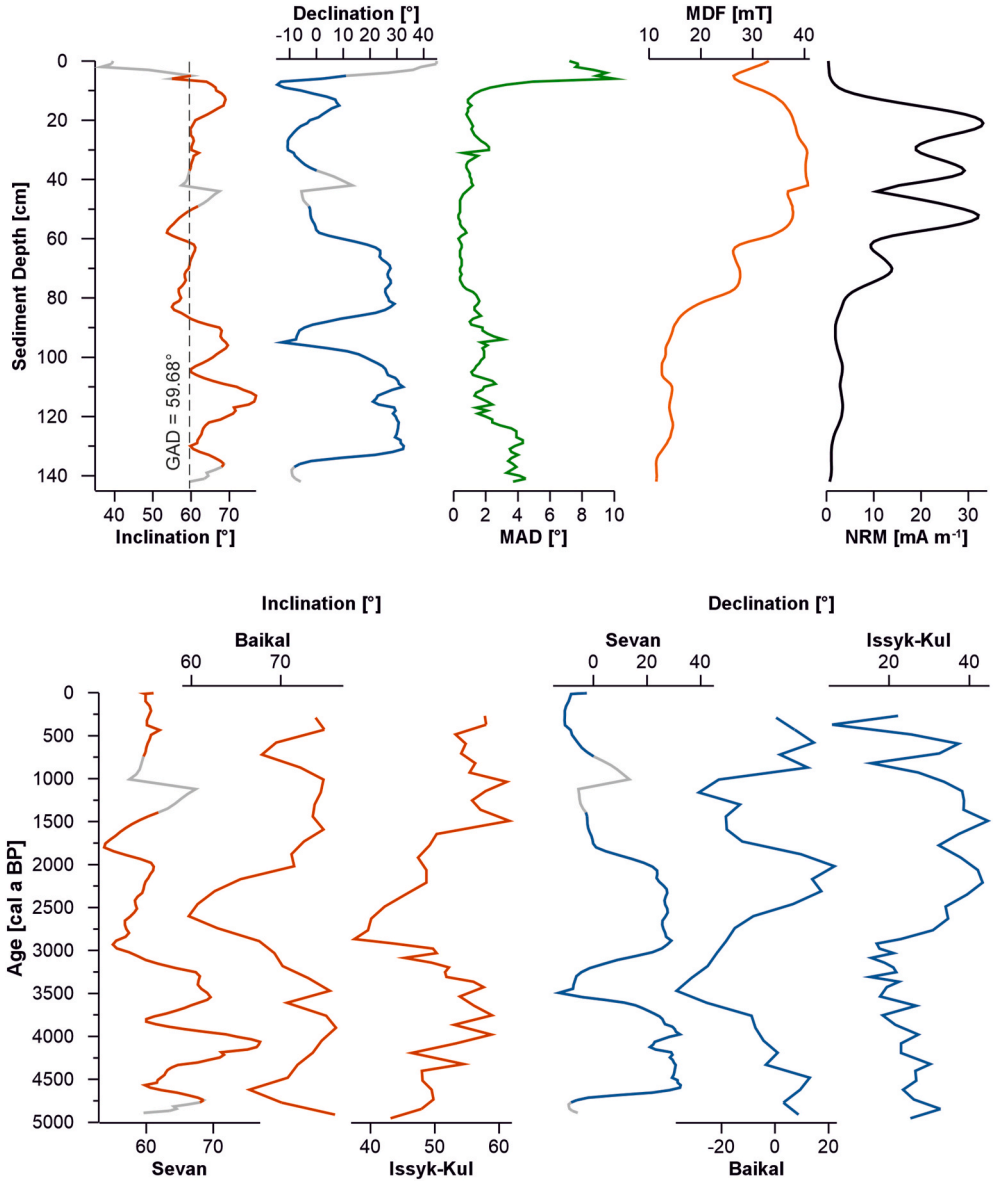

Fig. 4. Upper panel: Inclination, declination, maximum angular deviation (MAD) angles and median destructive fields (MDF) from principal component analysis as well as natural remanent magnetization (NRM) for sediment core SEV21-6 from Lake Sevan plotted on a depth scale. Please note that declination data are relative since the azimuth could not be controlled during coring.
Lower panel: Comparison of inclination and declination from Lake Sevan with records from Lakes Baikal (Peck et al., 1996) and Issyk-Kul (Gómez-Paccard et al., 2012).

comparison. Similar observations were recently made at archaeological sites in the Eastern Mediterranean where directions show significantly larger swings than existing field models leading to the conclusion that these models require substantial revision in this region (Ertepinar et al., 2020). Following this line of reasoning, it can be concluded that a reservoir effect cannot be postulated from our data, and that the chronology for the SEV21-6 record is robust resulting in a basal age of $4870^{+190}/_{-245}$ cal a BP (Fig. 3). The sedimentation rate in the radiocarbon dated lower part of the record is relatively low (0.2–0.4 mm a^{-1}) whereas in the uppermost part, the $^{137}Cs/^{210}Pb$ dated section, it is rather high reaching up to 3.4 mm a^{-1}. Assuming a hiatus between the two parts (as suggested by the $^{137}Cs/^{210}Pb$ data), the output of the chronological model suggests a hiatus of ~30 years with overlapping errors ($43^{+72}/_{-45}$ to $15^{+14}/_{-18}$ cal a BP) which is not detectable in the graphs presenting the measured parameters because of the short duration (e.g., Fig. 2).

4.3. Sedimentology and geochemistry

4.3.1. Indicators for environmental variations

Usually, minerogenic input to lacustrine systems is reflected by ideally inert elements such as Ti (Haberzettl et al. 2005, 2006). As in various other studies (Niemann et al., 2009; Ahlborn et al., 2015), here we also use Magnetic Susceptibility as well as K. As these minerogenic input indicators are often associated with fluvial input and hence precipitation (Kasper et al., 2021), they will be interpreted in this study accordingly, although other processes supplying minerogenic matter cannot be ruled out completely (Adolph et al., 2024). In addition to that, dilution processes cannot be excluded, i.e., dilution of minerogenic input by carbonate precipitation or vice versa (Kastner et al., 2010; Haberzettl et al., 2019). To check for this, we compared the correlation coefficients of minerogenic input indicators Ti and K with Ca (Table 3), which is representative for carbonates as it shows a similar pattern to quantitatively measured TIC in the individual lithological units (Fig. 2). High correlation coefficients are observed in laminated units A, B and E, which have high Ca and TIC values, whereas low correlation coefficients are found in units C and D where lower Ca and TIC predominate (Table 3). This indicates a dependency of one parameter on the other in laminated units A, B and E whereas this is not the case in non-laminated units C and D. Therefore, we assume that during units A, B and E the intensive carbonate precipitation dilutes the minerogenic input signal to a certain degree whereas in units C and D it can directly be used to reconstruct hydrological variability in the catchment. Although magnetic susceptibility is not compositional data and therefore not directly dependent on variations in Ca, calcite is a diamagnetic mineral and increased carbonate deposition will therefore also yield lowered magnetic susceptibility values (Haberzettl et al., 2010).

However, carbonate precipitation itself represented by Ca and TIC is also supposed to reflect lake level changes because increased deposition of $CaCO_3$ has been observed during and after the artificial modern lake level lowering of Lake Sevan (Alekin and Ulyanova, 1994). This can be observed in unit E of sediment core SEV21-6 (Fig. 2). An increased warming of the water, a lower evaporation rate and accelerated photosynthesis resulting from the increased abundance of diatoms, blue-green algae and green algae, decreased the concentrations of dissolved CO_2 and phosphate while increased terrigenous and autochthonous suspended matter caused centers of crystallization leading to a rapid carbonate precipitation (Alekin and Ulyanova, 1994). This carbonate precipitation is peaking in whiting events, which nowadays typically occur in October (Ulyanova, 1993). However, the top of unit E in SEV21-6 consists of much finer layers than the bottom of unit E (Fig. 2) potentially as a result of lake level stabilization and the slight rise of Lake Sevan after 2003 CE. Considering this mechanism, which occurs today during an anthropogenically induced lower lake level, we assume a similar mechanism under naturally lower lake level conditions in the past. We therefore suggest that a higher carbonate content reflects lower lake levels in general with thicker laminae representing a lake level lowering or lower lake level and thinner laminae a lake level stabilization.

Similar analogies between recent and past lake level lowerings are assumed for redox variations. In summer and fall, a cold water dome forms in Lake Sevan. In fall, the thermocline is deepening towards the bottom and the hypolimnion of the dome is isolated from the mixed water layers, which results in hypoxia (oxygen content <2 mg l^{-1}) (Gabrielyan et al., 2022). This is mirrored in the preservation of a lamination in some parts of the sediment sequence SEV21-6 and by a high Fe/Mn-ratio (Haberzettl et al., 2007). The dissolution of Mn compounds occurs if the redox potential (EH) decreases below 600 mV because of the reduction of Mn^{4+} to Mn^{2+} whereas the critical EH for the reduction of Fe^{3+} compounds to more soluble Fe^{2+} compounds is 100 mV (Sigg and Stumm, 1996). Therefore, if the redox potential drops to values between 100 and 600 mV, Fe/Mn-ratios will increase which can hence indicate reducing conditions (Haberzettl et al., 2007). Although it cannot be excluded that EH never dropped below 100 mV, the high correlation coefficient between the inert element Ti and Fe ($r = 0.92$) indicates that this is not the case. Consequently, a high Fe/Mn-ratio is interpreted as being indicative for reducing conditions. Of course, these mechanisms are amplified by modern anthropogenic effluents but already started when anthropogenic pollution was on a much lower level.

Grain sizes in such large lake systems have previously been interpreted to reflect paleoshoreline proximity with coarser grains representing a closer shoreline and therefore a lower lake level under natural conditions (Kasper et al., 2012). Similarly, lake level variations seem to be reflected by sedimentation rate. Sedimentation rate is assumed to be high during times of a closer shoreline resulting from a lower lake level enabling a reworking of easily erodible material, which was previously deposited subaquatiously. In addition to that, an increased carbonate precipitation during low lake levels adds to an increased sedimentation rate.

4.3.2. Environmental reconstruction

4.3.2.1. Unit A (141-125 cm/$4870^{+190}/_{-245}$ – $4420^{+320}/_{-360}$ cal a BP). High contributions of sand confirmed by coarse mean grain size values indicate a relatively close paleoshoreline and therefore a rather low lake level. This is supported by a high sedimentation rate (although the chronology is only based on few ages, Fig. 2). Alternations between dark and light-colored layers detected in the lithology are confirmed by (high-resolution) sedimentological data showing rapid high amplitude variations especially in established minerogenic input indicators such as Ti or *k* (dark layers) as well as in parameters representing carbonate precipitation such as Ca (light layers) (Fig. 2). This indicates the absence of bioturbation due to anoxic conditions similar to those observed at lower lake levels today. Such anoxic conditions are confirmed by relatively high Fe/Mn-ratios (Fig. 2). The lowest values in minerogenic input indicators (*k*, Ti, K) of the entire record might be the result of very dry conditions resulting in less fluvial input, although, a dilution by carbonate precipitation has to be considered. Due to the similarities with the lake level lowering, which occurred recently at Lake Sevan, we assume a lowering or low lake level during this unit.

Table 3
Determination coefficients of Ti/Ca and K/Ca for all lithological units.

Unit	Ti/Ca (R^2)	K/Ca (R^2)
E	0.61	0.45
D	0.42	0.14
C	0.28	0.03
B	0.60	0.37
A	0.82	0.52

4.3.2.2. Unit B (125-97 cm/4420$^{+320}/_{-360}$ – 3570$^{+135}/_{-115}$ cal a BP). Finer laminae as well as higher frequency variations in almost all parameters coupled with redox indicator Fe/Mn-ratio still indicating anoxic conditions (Fig. 2), point to a persisting low lake level with at least temporary anoxia in the hypolimnion. A low lake level is supported by still rather high carbonate contributions indicated by high Ca and TIC values and coarse grain sizes pointing to a close paleoshoreline (Fig. 2). Nevertheless, rising minerogenic input indicators might point to increased minerogenic input to a stabilized system potentially indicating somewhat more humid conditions in the catchment.

4.3.2.3. Unit C (97-75 cm/3570$^{+135}/_{-115}$ – 2560$^{+570}/_{-625}$ cal a BP). The absence of a distinct lamination together with partially lower Fe/Mn-ratios (Fig. 2) indicates more oxic bottom water conditions. Although minerogenic input indicators fluctuate on a similar level as in Unit B, carbonate indicators Ca and TIC are on a somewhat lower level and grain sizes (mean and sand) as well as sedimentation rate as paleoshoreline indicator decrease. This indicates wetter conditions with more erosion in the catchment and potentially a rising lake level.

4.3.2.4. Unit D (97-13 cm/2560$^{+570}/_{-625}$ – -19$^{+4}/_{-4}$ cal a BP = 1969$^{+4}/_{-4}$ CE). Low sedimentation rates and fine grain sizes (Fig. 2) point to a considerable increased shoreline distance of the coring location. The darker brown sediment color in this unit is mirrored by distinctly lower carbonate (Ca, TIC) precipitation. Ca and TIC show even a distinct low-value-interval around 64 cm (66-62 cm/2160$^{+635}/_{-535}$ to 1980$^{+590}/_{-490}$ cal a BP), which is not expressed in the other measured parameters, but might be related to the higher minerogenic input (especially *k*) starting at the bottom of unit D (*2560$^{+570}/_{-625}$* cal a BP) (Fig. 2). The high water supply indicated by minerogenic input might have resulted in a lake level rise and consequently in a first overflow of the lake system, which occurred frequently or continuously from that time on. At 52 cm sediment depth (1530$^{+290}/_{-290}$ cal a BP) highest values in all minerogenic input indicators are observed generally being on a higher level thereafter (especially *k*) (Fig. 2). This points to a very wet interval followed by generally moister conditions keeping the lake level high.

4.3.2.5. Unit E (13-0 cm/-19$^{+4}/_{-4}$ cal a BP – -71 cal a BP = 1969$^{+4}/_{-4}$ CE – 2021CE). Unit E seems to be dominated by the results of anthropogenic impact. Due to the artificial lake level lowering, carbonate precipitation shifts to an unprecedented level distinctly diluting minerogenic input (Fig. 2). Considering the previous grain size history, coarser grains would have to be assumed. However, this is not the case and in contrast to previous observations grains become even finer (Fig. 2). This is probably due to the fact that during the lake level lowstand in units A and B, the sediment cover of the exposed areas was not thick enough and coarser grains could be eroded during that time. In contrast, now in unit E, exposed areas have been water-covered for an extended time (at least unit D, potentially also unit C) and previously accumulated sediments can be reworked and transported into more distal parts of the lake. Nevertheless, as expected with a lower lake level, sedimentation rate increases drastically and bottom water becomes anoxic as indicated by the highest Fe/Mn-ratios of the record and the formation of laminae (Fig. 2). Although the lake level lowering started in the 1930s, sedimentological evidence only starts in 1969$^{+4}/_{-4}$ CE. This might be due to larger uncertainties than expected in the chronology, a hysteresis of the lake system or a threshold that needed to be passed.

In summary, the sediment sequence SEV21-6 records a long-term lake level rise of Lake Sevan with light fluctuations from the bottom of the record at 4870$^{+190}/_{-245}$ cal a BP to the 1930s when the lake level was lowered artificially. These modern lower lake level conditions can be used as a modern analog for older intervals of the sequence.

4.3.3. Cyclic behavior of minerogenic input indicators

In addition to the rhythmicity visually observed in units A and B triggered by carbonate precipitation, minerogenic input indicators show longer periodicities. While these do not reach statistical significance probably due to a combination of a short record and an imperfect age model, we discuss these here. A 2600 to 2200 year periodicity (Fig. 5) might reflect the Hallstatt oscillation with a periodicity of 2500 to 2100 (Scafetta et al., 2016), about 2200 (Steinhilber et al., 2012), ~2400 (Usoskin et al., 2016) or 2310 ± 304 years (Fletcher et al., 2024). The origin of the Hallstatt cycle is still debated and may be related to solar activity (Usoskin et al., 2016; Usoskin, 2023), changes in the dipole moment of the magnetic field (Dergachev and Vasiliev, 2019) or an astronomic origin (Scafetta et al., 2016). Here, two Hallstatt cycles may be observed, which is not enough for a robust analysis due to the shortness of the time interval of this study.

Considering uncertainties in the chronology, a shorter periodicity of ~1000 to 600 years in SEV21-6 (Fig. 5) is similar to Eddy cycles (Abreu et al., 2010) with a periodicity of 1050 to 900 (Scafetta et al., 2016), around 1000 (Steinhilber et al., 2012), 980 (Abreu et al., 2010) or 976 ± 53 years (Fletcher et al., 2024). As the sun is not the only driver of the climate system other forcing factors and complex interactions might have changed the effects on climate (Steinhilber et al., 2012). However, similar to our study, Eddy cycle variations in other studies are unstable and not statistically significant either (Biswas et al., 2023; Usoskin, 2023). Other studies also highlight that amplitudes of cycles have varied in time (Fletcher et al., 2024).

The maximum of the Hallstatt cycle in radiocarbon data (minimum total solar irradiance) corresponds to about 1645 CE, namely the beginning of the Maunder Minimum (1645–1715 CE) (Scafetta et al., 2016). This is contemporaneous to a reduced minerogenic input to Lake Sevan, which characterizes the minimum in the 2600- to 2200-year filter as well as the 1000-600-year filter, indicating that these periodicities may have amplified each other at this point in time. This is supported by the fact that grand solar minima and maxima occurred intermittently clustering near lows and highs of the Hallstatt cycle (Usoskin et al., 2016). However, the mechanism behind the detailed relationship of minerogenic input to Lake Sevan and solar variations has to be explored in future studies on longer timescales.

5. Discussion

Hydrological variations as indicated in the parameters from sediment core SEV21-6 are supported by various investigations in the catchment of Lake Sevan. Outcrops (e.g., Dzknaget or Norashen, Fig. 1) (Vardanyan et al., 2018; Gorbatov et al., 2019) and archaeological remains exposed after the modern artificial lake level lowering on the Artanish peninsula (Hovhannisyan et al., 2023) testify previous lake level high- and low stands. In addition to that, investigations on peat bogs such as the Vanevan wetland (Robles et al., 2022) or Tsovinar (Hayrapetyan et al., 2023) in the southeastern part of Lake Sevan (Fig. 1) show a similar hydrological history (Fig. 6).

5.1. Unit A (141-125 cm/4870$^{+190}/_{-245}$ – 4420$^{+320}/_{-360}$ cal a BP)

A lake level low stand as indicated in the parameters from sediment core SEV21-6 between 4870$^{+190}/_{-245}$ and 4420$^{+320}/_{-360}$ cal a BP is supported by cultural anthropogenic horizons with archaeological remains above a lacustrine section indicative for a high lake level dated to 7170$^{+250}/_{-270}$ cal a BP (6270 ± 110 BP, MGU-215, Table 4) in the Norashen outcrop (Vardanyan et al., 2018; Gorbatov et al., 2019) (see Fig. 1 for location). These archaeological horizons have been dated to the 3rd and the middle of the 2nd millennium BCE (Vardanyan et al., 2018) supporting the interpretation of a low lake level for units A and B. Additional support for a low lake level of Lake Sevan after 4800 cal a BP comes from the Vanevan wetland (Robles et al., 2022) for which a drying phase (decrease in precipitation) is recorded between 5100 and 4800 cal a BP, transforming a lacustrine environment to a peatland at 4800 cal a BP. This trend agrees with records in Georgia and Central Asia

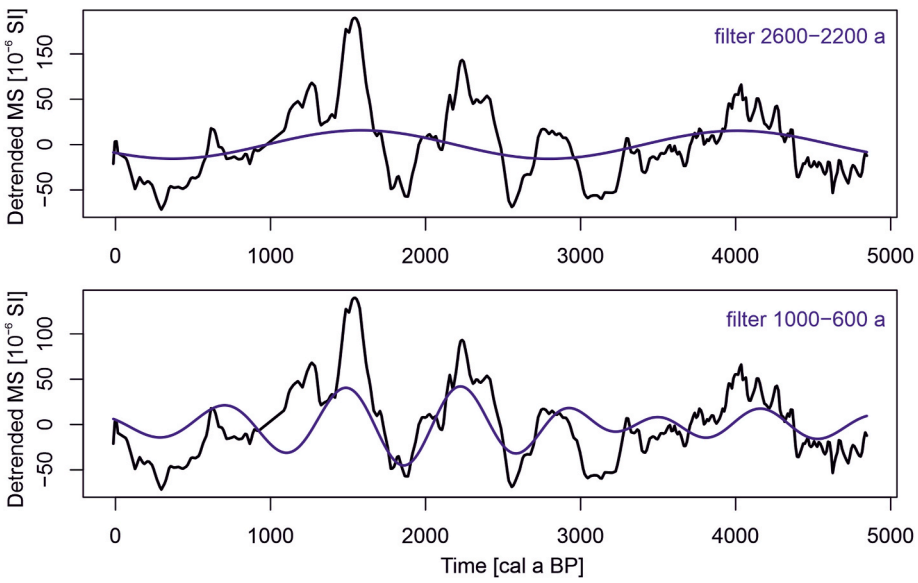

Fig. 5. Comparison of linearly detrended magnetic susceptibility signals normalized to a mean of zero (ordinates) vs. time (abscissa). The magnetic susceptibility datasets are plotted in black, two Taner filters (Taner, 1992) are plotted together with the data in blue, extracting the components from 2600 to 2200 years (top) and 1000-600 years (bottom).

which also show decreasing precipitation (Robles et al., 2022). The water level remains low in the Vanevan peat until 4500 cal a BP when semi-aquatic vegetation developed (Robles et al., 2022) which is in line with somewhat more humid conditions in SEV21-6 at the transition from unit A to unit B at $4420^{+320}/_{-360}$ cal a BP.

5.2. Unit B (125-97 cm/$4420^{+320}/_{-360}$ – $3570^{+135}/_{-115}$ cal a BP)

The generally still low lake level at Lake Sevan in unit B coincides with archaeological findings in the Lchashen section dated to $3950^{+285}/_{-305}$ (3630 ± 100 a BP, MGU-OAN-29) and $3770^{+305}/_{-280}$ cal a BP (3500 ± 100 a BP, MGU-OAN-30, both Table 4) testifying a low lake level (Aslanian, 1984). A still rather low water level is also found at the Vanevan wetland. Although, this phase is associated with the 4.2 ka arid event lasting from 4200 to 3700 cal a BP there (Robles et al., 2022).

5.3. Unit C (97- 75 cm/$3570^{+135}/_{-115}$ – $2560^{+570}/_{-625}$ cal a BP)

The wetter conditions and a lake level rise in Unit C are supported by a radiocarbon age of $3390^{+310}/_{-385}$ cal a BP (3180 ± 130 a BP, MGU-251, Table 4) in lacustrine sediments some centimeters above an archaeological horizon in the Norashen outcrop (Vardanyan et al., 2018; Gorbatov et al., 2019). This is in contrast to a stone with cuneiform dating to 2735-2710 cal a BP (note that original age is given as 785-760 BC and was recalculated to cal a BP for comparison with other data) found during excavations at Lchashen (Aslanian, 1984). This either implies that the stone with the cuneiform was either at a higher elevation still above the lake level at that time or a lake level lowering occurred again after $3390^{+310}/_{-385}$ cal a BP. Both would be conceivable according to our data. However, according to archaeological data from the Artanish peninsula a lake level rise is inferred between $2940^{+115}/_{-75}$ and $2580^{+135}/_{-90}$ cal a BP (recalibrated 2837 ± 22 and 2943 ± 21 a BP, MAMS 43487 and MAMS 43488, Table 4) (Avagyan et al., 2023; Hovhannisyan et al., 2023) which would indicate centennial-scale lake level variations.

Although the median age of $3710^{+120}/_{-125}$ cal a BP (3450 ± 35 a BP, Poz-52,962 (Joannin et al., 2022), Table 4) for the formation of neighboring Kalavan Red Lake is somewhat older than the beginning of unit C, the error of the chronologies/datings are clearly overlapping. The landslide forming this lake is related to a combination of slope steepness, tectonic activity, and water saturation in the substratum (Joannin et al., 2022), the latter perfectly matching a shift toward wetter conditions in unit C. However, the water level of the Vanevan wetland south of Lake Sevan remains low at the beginning of unit C.

5.4. Unit D (97-13 cm/$2560^{+570}/_{-625}$ – $-19^{+4}/_{-4}$ cal a BP = $1969^{+4}/_{-4}$ CE)

Similar to the results from sediment core SEV21-6 a high lake level is testified by radiocarbon ages in lacustrine sediments in the Norashen section dating to $2060^{+245}/_{-215}$ (2090 ± 70 a BP, MGU-244) and $1970^{+340}/_{-260}$ cal a BP (2020 ± 120 a BP, MGU-245, Table 4) (Vardanyan et al., 2018) as well as an age on wood of $940^{+425}/_{-410}$ (1010 ± 250 a BP, MGU-IOAN-178) and shells of $880^{+400}/_{-335}$ cal a BP (940 ± 220 a BP, MGU-55) in lacustrine sediments distinctly above alluvial material in the Dzknaget outcrop (Sayadyan et al., 1974; Gorbatov et al., 2019).

South of Lake Sevan, the water level rises at 2300 to 1800 cal a BP at Vanevan (Robles et al., 2022) and from 2050 to 1750 cal a BP (100 BC to AD 200 in the original publication) at Tsovinar (Hayrapetyan et al., 2023). Subsequently, the water level stayed high at Tsovinar (Hayrapetyan et al., 2023) which is in agreement with our record. Unfortunately, after 2300 cal a BP a modified vegetation structure due to human activities influences the paleoclimate reconstructions at the Vanevan wetland. Therefore, according to the authors of this study climate reconstructions for this period are not reliable (Robles et al., 2022) and cannot be compared to our reconstructions. Nevertheless, the water level rise from 2300 to 1800 cal a BP at Vanevan is contemporaneous with the Ca minimum between 66 and 62 cm ($2160^{+635}/_{-535}$ to $1980^{+590}/_{-490}$ cal a BP) and the preceding minerogenic input in SEV21-6 indicating a freshwater pulse during this time. Roughly at the same time (2000-1600 cal a BP) erosive activity returned to the catchment of Kalavan Red Lake (Joannin et al., 2022) potentially also pointing to an intensified precipitation interval around 2000 cal a BP.

5.5. Unit E (13-0 cm/$-19^{+4}/_{-4}$ cal a BP – -71 cal a BP = $1969^{+4}/_{-4}$ CE – 2021 CE)

The input of smaller grains to Unit D is confirmed by observations in the littoral areas where sandy-oozy matter, that accumulated before the

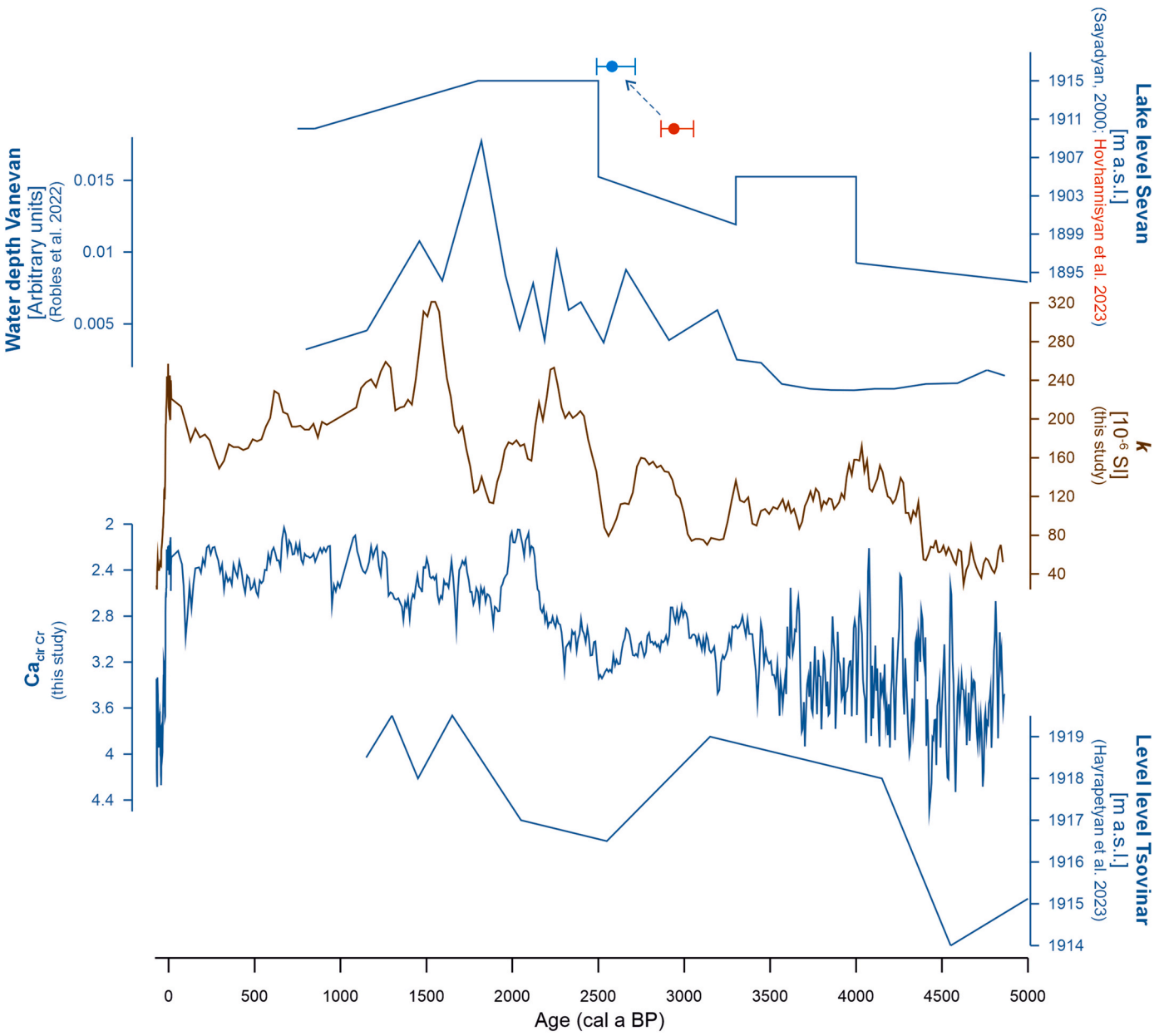

Fig. 6. Lake level reconstructions from Lake Sevan: From top to bottom: Lake level reconstructions from outcrops (Sayadyan, 2000) and archaeological artifacts (Hovhannisyan et al., 2023) (note that the two ages shown from Hovhannisyan et al. (2023) are recalibrated median ages of the 2-sigma distribution (Table 4)), water depth variations from Vanevan peat bog (Robles et al., 2022), Magnetic Susceptibility (*k*) as indicator for minerogenic input reflecting hydrological variations in the catchment (this study), center-log-ratio transformed XRF-scanning based Calcium ($Ca_{clr\ Cr}$) measured with a Cr-tube (this study) reflecting lake level variations and lake level reconstruction from Tsovinar-1 peat section (Hayrapetyan et al., 2023).

decrease of the lake level, is subjected to intensive erosion. This has increased the supply of minute oozy fractions into the water masses (Legovich et al., 1973) and ultimately to the distal site of SEV21-6.

Potentially additional climate variations occurred as described in other studies from Armenia (Joannin et al., 2022). However, if present, these variations were not severe enough to influence the distal sediments from Small Sevan or were overprinted by the artificial lake level lowering.

5.6. Lake level reconstruction for the past 5000 years

Unfortunately, it is not possible to determine exact water level elevations in our study or for most archaeological remains found in literature. Nevertheless, more recent studies tried to quantify lake level-variations (Hayrapetyan et al., 2023). Those studies often obtained different magnitudes of change but trends mostly coincide and result in a coherent picture for the catchment of Lake Sevan (Fig. 6).

As other studies (Vardanyan et al., 2018; Gorbatov et al., 2019; Avagyan et al., 2023) suggest a distinctly higher lake level of Lake Sevan (at least at a similar elevation as before the anthropogenic lowering in modern times) before the time slice covered by sediment core SEV21-6, we suggest a climatic control on lake level variations rather than geomorphologic/tectonic processes. This supports the conclusions of Gorbatov et al. (2019) and Hayrapetyan et al. (2023) that the main factor determining the fluctuations in the level of Lake Sevan in the Holocene is climatic although tectonic influences cannot be excluded. This would shift the timing of the damming of the Hrazdan River to a time frame before $4870^{+190}/_{-245}$ cal a BP.

Interestingly, studies beyond the catchment further to the northwest as for example the mire site of Shenkani (Cromartie et al., 2020) or

Table 4
Recalibrated radiocarbon ages mentioned in the text (Sayadyan et al., 1974; Aslanian, 1984; Vardanyan et al., 2018; Gorbatov et al., 2019; Hovhannisyan et al., 2023) using the SHCal20 calibration data set (Hogg et al., 2020) in the online version of the Calib 8.2 software (Stuiver et al., 2020).

Site	Conventional Radiocarbon Age (a BP)	Error (a)	Median calibrated age (cal a BP)	Error + (a)	Error - (a)	Material	Laboratory Number	Reference
Norashen	6270	110	7170	250	270	Mollusk shells of Limnaea stagnalis (L.), Radix ovate (Drap.), *Planorbis planorbis* (L.), Gyraulus laevis (Alder), Pisidium casertanum (Poli), Succinea obionga (Drap.)	MGU-215	Gorbatov et al., (2019), Vardanyan et al., (2018)
Norashen	3180	130	3390	310	385	Mollusk shells of Limnaea stagnalis (L.), Radix suricularia (L.), Valvata piscinalis (Mull), *Planorbis planorbis* (L.) Pisidium casertanum (Poli), *Succinea putris* (L.)	MGU-251	Gorbatov et al., (2019), Vardanyan et al., (2018)
Norashen	2020	120	1970	340	260		MGU-245	Gorbatov et al., (2019), Vardanyan et al., (2018)
Norashen	2090	70	2060	245	215		MGU-244	Gorbatov et al., (2019), Vardanyan et al., (2018)
Dzknaget	1010	250	940	425	410	Wood	MGU-IOAN-178	Gorbatov et al., (2019), Sayadyan et al., (1974)
Dzknaget	940	220	880	400	335	Mollusk shells of *Planorbis planorbis* (L.), Limnaea auricularia, L. glutinosa, *L. stagnalis*	MGU-55	Gorbatov et al., (2019), Sayadyan et al., (1974)
Lchashen	3500	100	3770	305	280	Chariot wood	MGU-OAN-29	Aslanian (1984)
Lchashen	3630	100	3950	285	305	Chariot wood	MGU-OAN-30	Aslanian (1984)
Artanish	2837	22	2940	115	75	Human bone	MAMS 43487	Hovhannisyan et al. (2023)
Artanish	2493	21	2580	135	90	Human bone	MAMS 43488	Hovhannisyan et al. (2023)

Zarishat fen (Joannin et al., 2014), do not show a similarly coherent picture. Reasons for the differences between these sites and the Lake Sevan catchment will have to be further explored in the future.

5.7. Future

Model calculations from the 90s indicate that the lake level of Lake Sevan which was at 1897 m asl at that time should be raised at least by 6 m (1903 m asl) to restore the hypolimnion and the oxygen regime (Hovanesian and Bronozian, 1994). This is in the same range as earlier estimates of 7 m to 1906 m asl (based on a lake level at an elevation at 1899 m asl) which were assumed to bring back its previous oligotrophic state (Legovich et al., 1973). Although the lake level already increased somewhat since that time, this would require an additional lake level rise of 3–6 m based on today's level at 1900 m asl. These results are confirmed by our investigations on SEV21-6 showing that under natural conditions anoxic conditions caused by lake level low stands can vanish if the lake level is rising.

6. Conclusions

With respect to hydrological variations, the here presented first investigations on distal sediments from Lake Sevan reveal a coherent picture with investigations in the immediate surrounding of the lake but with the advantage of a much higher resolution. Taking advantage of the "modern analog" of the artificial 20th-century lake level lowering, a preceding naturally induced lake level lowering could be reconstructed. Sediments of core SEV21-6 reflect a reflooding of the Sevan basin from $4870^{+190}/_{-245}$ cal a BP onward until the beginning of the artificial lowering. A distinct shift towards wetter conditions is observed between 2500 and 2000 cal a BP resulting in a very high lake level.

This study shows that under natural conditions the lake can recover from an oxygen deficit if the lake level rises. Superimposed on this long-term lake level rise, variations in minerogenic input indicate additional hydrological variations which might be attributed to the Hallstatt and Eddy cycles. However, processes and causes for this relationship need to be further explored on longer time scales in future. Paleomagnetic secular variation data from Lake Sevan agree well with distant sites to the northeast but disagree with sites closer to the southwest. This might be due to an influence of the Levantine Iron Age geomagnetic Anomaly (LIAA) but also here details need to be further explored in the future.

CRediT authorship contribution statement

Torsten Haberzettl: Conceptualization, Data curation, Formal analysis, Funding acquisition, Investigation, Methodology, Project administration, Resources, Validation, Visualization, Writing – original draft, Writing – review & editing. **Marie-Luise Adolph:** Data curation, Formal analysis, Investigation, Methodology, Validation, Visualization, Writing – review & editing. **Taron Grigoryan:** Validation, Writing – review & editing. **Hayk Hovakimyan:** Validation, Writing – review & editing. **Thomas Kasper:** Methodology, Validation, Writing – review & editing. **Norbert Nowaczyk:** Data curation, Formal analysis, Investigation, Resources, Writing – review & editing. **Christian Zeeden:** Formal analysis, Investigation, Validation, Visualization, Writing – review & editing. **Lilit Sahakyan:** Funding acquisition, Investigation, Project administration, Validation, Writing – review & editing.

Declaration of competing interest

The authors declare that they have no known competing financial interests or personal relationships that could have appeared to influence the work reported in this paper.

Data availability

Data will be made available on request.

Acknowledgments

We would like to acknowledge the helping hands of U. Dolgner and U. Amelung during TIC, grain size and paleomagnetic measurements. T.

Grigoryan and H. Hovakimyan received a DAAD fellowship within the Leonhard-Euler program for a research stay in Greifswald to contribute to this manuscript. The Armenian team was also supported by the State base funding. We would like to thank P.G. Appleby and G.T. Piliposian for Cs/Pb-dating, C. Ohlendorf and R. Stiens for XRF scanning and N. Hayrapetyan as well as S. Joannin for providing data from Tsovinar and Vanevan for comparison. Finally, we would like to thank M. Schultze, R. Kunze and A. Avagyan for discussions and sharing their results.

References

Abreu, J.A., Beer, J., Ferriz-Mas, A., 2010. Past and Future Solar Activity from Cosmogenic Radionuclides. SOHO-23: Understanding a Peculiar Solar Minimum, vol. 428. ASP Conference Series. Cranmer, S.R., J.T. Hoeksema, J.L. Kohl, pp. 287–295.

Acopian Center for the Environment, 2018. Vector database Armenia. Series Vector Database Armenia Edition. http://www.acopiancenter.am/GISPortal/. (Accessed 27 August 2024).

Adolph, M.L., Czerwinski, S., Dreßler, M., Strobel, P., Bliedtner, M., Lorenz, S., Debret, M., Haberzettl, T., 2024. North Atlantic Oscillation polarity during the past 3 ka derived from lacustrine sediments of large lowland lake Schweriner See, NE-Germany. Clim. Past 2023, 1–39. https://doi.org/10.5194/cp-2023-73.

Ahlborn, M., Haberzettl, T., Wang, J., Alivernini, M., Schlütz, F., Schwarz, A., Su, Y., Frenzel, P., Daut, G., Zhu, L., Mäusbacher, R., 2015. Sediment dynamics and hydrologic events affecting small lacustrine systems on the southern-central Tibetan Plateau - the example of TT Lake. Holocene 25 (3), 508–522. https://doi.org/10.1177/0959683614561885.

Alekin, O.A., Ulyanova, D.S., 1994. Characteristics of present-day carbonate generation in Lake Sevan. Transactions of the Russian Academy of Sciences 326 (7), 182–185.

Appleby, P.G., 2001. Chronostratigraphic techniques in recent sediments. In: Last, W.M., Smol, J.P. (Eds.), Tracking Environmental Change Using Lake Sediments. Volume 1: Basin Analysis, Coring, and Chronological Techniques. Kluwer Academic, Dordrecht, pp. 171–203.

Appleby, P.G., Oldfield, F., 1978. The calculation of ^{210}Pb dates assuming a constant rate of supply of unsupported ^{210}Pb to the sediment. Catena 5, 1–8.

Appleby, P.G., Nolan, P.J., Gifford, D.W., Godfrey, M.J., Oldfield, F., Anderson, N.J., Battarbee, R.W., 1986. ^{210}Pb dating by low background gamma counting. Hydrobiologia 141, 21–27.

Appleby, P.G., Richardson, N., Nolan, P.J., 1991. ^{241}Am dating of lake sediments. Hydrobiologia 214, 35–42.

Appleby, P.G., Richardson, N., Nolan, P.J., 1992. Self-absorption corrections for well-type germanium detectors. Nucl. Instrum. Methods Phys. Res. Sect. B Beam Interact. Mater. Atoms 71, 228–233.

Aslanian, A.T., 1984. The Armenian Soviet Socialist Republic Excursions: 010 Neotectonics of Armenia: 102 Permian and Triassic Deposits of the Transcaucasus: Guide Book for the 27th International Geological Congress. Department of Geology of the Armenian SSR.

Avagyan, A., Sahakyan, L., Meliksetian, K., Karakhanyan, A., Lavrushin, V., Atalyan, T., Hovakimyan, H., Avagyan, S., Tozalakyan, P., Shalaeva, E., Chatainger, C., Sokolov, S., Sahakov, A., Alaverdyan, G., 2020. New evidences of Holocene tectonic and volcanic activity of the western part of Lake Sevan (Armenia). Geol. Q. 64 (2), 288–303. https://doi.org/10.7306/gq.1530.

Avagyan, A., Sahakyan, L., Meliksetyan, K., Hovhannisyan, A., Arakelyan, D., Galoyan, G., Melik-Adamyan, H., Grigoryan, T., Sahakyan, K., Grigoryan, E., Avagyan, S., Safaryan, R., 2023. The potential for a geohazard-related geopark in Armenia. Geoheritage 15 (4), 133. https://doi.org/10.1007/s12371-023-00900-2.

Biswas, A., Karak, B.B., Usoskin, I., Weisshaar, E., 2023. Long-term modulation of solar cycles. Space Sci. Rev. 219 (3), 19. https://doi.org/10.1007/s11214-023-00968-w.

Blaauw, M., Christen, J.A., 2011. Flexible paleoclimate age-depth models using an autoregressive gamma process. Bayesian Analysis 6 (3), 457–474.

Blott, S.J., Pye, K., 2001. GRADISTAT: a grain size distribution and statistics package for the analysis of unconsolidated sediments. Earth Surf. Process. Landforms 26 (11), 1237–1248. https://doi.org/10.1002/esp.261.

Cromartie, A., Blanchet, C., Barhoumi, C., Messager, E., Peyron, O., Ollivier, V., Sabatier, P., Etienne, D., Karakhanyan, A., Khatchadourian, L., Smith, A.T., Badalyan, R., Perello, B., Lindsay, I., Joannin, S., 2020. The vegetation, climate, and fire history of a mountain steppe: a Holocene reconstruction from the South Caucasus, Shenkani, Armenia. Quat. Sci. Rev. 246, 106485 https://doi.org/10.1016/j.quascirev.2020.106485.

Dergachev, V.A., Vasiliev, S.S., 2019. Long-term changes in the concentration of radiocarbon and the nature of the Hallstatt cycle. J. Atmos. Sol. Terr. Phys. 182, 10–24. https://doi.org/10.1016/j.jastp.2018.10.005.

Ertepinar, P., Hammond, M.L., Hill, M.J., Biggin, A.J., Langereis, C.G., Herries, A.I.R., Yener, K.A., Akar, M., Gates, M.H., Harrison, T., Greaves, A.M., Frankel, D., Webb, J. M., Özgen, İ., Yazicioglu, G.B., 2020. Extreme geomagnetic field variability indicated by Eastern Mediterranean full-vector archaeomagnetic records. Earth Planet Sci. Lett. 531, 115979 https://doi.org/10.1016/j.epsl.2019.115979.

Fletcher, W.J., Sánchez Goñi, M.F., Naughton, F., Seppä, H., 2024. Chapter 9 - synthesis and perspectives: drivers, rhythms, and spatial patterns of Holocene climate change. In: Palacios, D., Hughes, P.D., Jomelli, V., Tanarro, L.M. (Eds.), European Glacial Landscapes. Elsevier, pp. 127–146. https://doi.org/10.1016/B978-0-323-99712-6.00026-X.

Gabrielyan, B., Khosrovyan, A., Schultze, M., 2022. A review of anthropogenic stressors on Lake Sevan. Armenia. Journal of Limnology 81 (s1), 2061. https://doi.org/10.4081/jlimnol.2022.2061.

Gevorgyan, G., von Tuempling, W., Shahnazaryan, G., Friese, K., Schultze, M., 2022. Lake-wide assessment of trace elements in surface sediments and water of Lake Sevan. J. Limnol. 81 (s1), 2096. https://doi.org/10.4081/jlimnol.2022.2096.

Ginsberg, A., 1929. A geological and petrographical description of the north-eastern shore of Lake Gokcha. In: Loewinson-Lessing, F. (Ed.), Le Bassin du lac Sevan (Goktcha): Résultats scientifiques de l'expédition de 1927/Bassejn ozera Sevan (Gokča), pp. 507–509. Leningrad.

Gómez-Paccard, M., Larrasoaña, J.C., Giralt, S., Roberts, A.P., 2012. First paleomagnetic results of mid- to late Holocene sediments from Lake Issyk-Kul (Kyrgyzstan): Implications for paleosecular variation in central Asia. Geochemistry, Geophyics, Geosystems 13 (3), Q03019. https://doi.org/10.1029/2011GC004015.

Gorbatov, E.S., Vardanyan, A.A., Korzhenkov, A.M., Razumniy, S.D., 2019. Lake Sevan (Armenia) Deposits as indicator of paleoclimate and neotectonic processes. Izvestiya Atmos. Ocean. Phys. 55 (8), 860–869. https://doi.org/10.1134/S0001433819080048.

Gulakyan, S.Z., Wilkinson, I.P., 2002. The influence of earthquakes on large lacustrine ecosystems, with particular emphasis on Lake Sevan, Armenia. Hydrobiologia 472 (1–3), 123–130. https://doi.org/10.1023/A:1016398420530.

Haberzettl, T., Fey, M., Lücke, A., Maidana, N., Mayr, C., Ohlendorf, C., Schäbitz, F., Schleser, G.H., Wille, M., Zolitschka, B., 2005. Climatically induced lake level changes during the last two millennia as reflected in sediments of Laguna Potrok Aike, southern Patagonia (Santa Cruz, Argentina). J. Paleolimnol. 33 (3), 283–302. https://doi.org/10.1007/s10933-004-5331-z.

Haberzettl, T., Wille, M., Fey, M., Janssen, S., Lücke, A., Mayr, C., Ohlendorf, C., Schäbitz, F., Schleser, G.H., Zolitschka, B., 2006. Environmental change and fire history of southern Patagonia (Argentina) during the last five centuries. Quat. Int. 158, 72–82. https://doi.org/10.1016/j.quaint.2006.05.029.

Haberzettl, T., Corbella, H., Fey, M., Janssen, S., Lücke, A., Mayr, C., Ohlendorf, C., Schäbitz, F., Schleser, G.H., Wille, M., Wulf, S., Zolitschka, B., 2007. Lateglacial and Holocene wet-dry cycles in southern Patagonia: chronology, sedimentology and geochemistry of a lacustrine record from Laguna Potrok Aike, Argentina. Holocene 17 (3), 297–310. https://doi.org/10.1177/0959683607076437.

Haberzettl, T., St-Onge, G., Lajeunesse, P., 2010. Multi-proxy records of environmental changes in Hudson Bay and Strait since the final outburst flood of Lake Agassiz–Ojibway. Mar. Geol. 271 (1), 93–105. https://doi.org/10.1016/j.margeo.2010.01.014.

Haberzettl, T., Henkel, K., Kasper, T., Ahlborn, M., Su, Y., Wang, J., Appel, E., St-Onge, G., Stoner, J., Daut, G., 2015. Independently dated paleomagnetic secular variation records from the Tibetan Plateau. Earth Planet Sci. Lett. 416, 98–108. https://doi.org/10.1016/j.epsl.2015.02.007.

Haberzettl, T., Kirsten, K.L., Kasper, T., Franz, S., Reinwarth, B., Baade, J., Daut, G., Meadows, M.E., Su, Y.L., Mäusbacher, R., 2019. Using ^{210}Pb-data and paleomagnetic secular variations to date anthropogenic impact on a lake system in the Western Cape, South Africa. Quat. Geochronol. 51, 53–63. https://doi.org/10.1016/j.quageo.2018.12.004.

Haberzettl, T., Kasper, T., Stoner, J.S., Rahobisoa, J.J., Daut, G., 2021. Extending and refining the paleomagnetic secular variation database for south-eastern Africa (Madagascar) to 2500 cal BP. Earth Planet Sci. Lett. 565 https://doi.org/10.1016/j.epsl.2021.116931.

Hayrapetyan, N., Hakobyan, E., Kvavadze, E., Martinetto, E., Gabrielyan, I., Bruch, A.A., 2023. Middle to late Holocene lake level changes of Lake Sevan (Armenia) – evidence from macro and micro plant remains of Tsovinar-1 peat section. Quat. Int. 661, 34–48. https://doi.org/10.1016/j.quaint.2023.03.013.

Hogg, A.G., Heaton, T.J., Hua, Q., Palmer, J.G., Turney, C.S.M., Southon, J., Bayliss, A., Blackwell, P.G., Boswijk, G., Bronk Ramsey, C., Pearson, C., Petchey, F., Reimer, P., Reimer, R., Wacker, L., 2020. SHCal20 southern hemisphere calibration, 0–55,000 Years cal BP. Radiocarbon 62 (4), 759–778. https://doi.org/10.1017/RDC.2020.59.

Hovanesian, R., Bronozian, H., 1994. Restoration and management of Lake Sevan in Armenia: Problems and prospects. Lake Reservoir Manag. 9 (1), 178–182.

Hovhannisyan, A., Bobokhyan, A., Kunze, R., Fassbinder, J.W.E., Hahn, S.E., Arakelyan, D., Grigoryan, A., Harutyunyan, M., Siradeghyan, V., 2023. Geoarchaeological investigations in Artanish Peninsula, Armenia: testing a new geochemical prospecting method for archaeology. Archaeol. Prospect. 31 (1), 3–22. https://doi.org/10.1002/arp.1917.

Jarvis, A., Reuter, H.I., Nelson, A., Guevara, E., 2008. Hole-filled seamless SRTM data V4. International Centre for Tropical Agriculture (CIAT). From: https://srtm.csi.cgiar.org.

Jenderedjian, K., Hakobyan, S., Stapanian, M.A., 2012. Trends in benthic macroinvertebrate community biomass and energy budgets in Lake Sevan, 1928–2004. Environ. Monit. Assess. 184 (11), 6647–6671. https://doi.org/10.1007/s10661-011-2449-0.

Joannin, S., Ali, A.A., Ollivier, V., Roiron, P., Peyron, O., Chevaux, S., Nahapetyan, S., Tozalakyan, P., Karakhanyan, A., Chataigner, C., 2014. Vegetation, fire and climate history of the Lesser Caucasus: a new Holocene record from Zarishat fen (Armenia). J. Quat. Sci. 29 (1), 70–82. https://doi.org/10.1002/jqs.2679.

Joannin, S., Capit, A., Ollivier, V., Bellier, O., Brossier, B., Mourier, B., Tozalakian, P., Colombié, C., Yevadian, M., Karakhanyan, A., Gasparyan, B., Malinsky-Buller, A., Chataigner, C., Perello, B., 2022. First pollen record from the late Holocene forest environment in the lesser Caucasus. Rev. Palaeobot. Palynol. 304, 104713 https://doi.org/10.1016/j.revpalbo.2022.104713.

Karakhanyan, A., Arakelyan, A., Avagyan, A., Sadoyan, T., 2017. Aspects of the seismotectonics of Armenia: new data and reanalysis. In: Sorkhabi, R. (Ed.), Tectonic Evolution, Collision, and Seismicity of Southwest Asia: in Honor of Manuel

Berberian's Forty-Five Years of Research Contributions. Geological Society of America. https://doi.org/10.1016/j.revpalbo.2022.104713.
Kasper, T., Haberzettl, T., Doberschütz, S., Daut, G., Wang, J., Zhu, L., Nowaczyk, N., Mäusbacher, R., 2012. Indian Ocean Summer Monsoon (IOSM)-dynamics within the past 4 ka recorded in the sediments of Lake Nam Co, central Tibetan Plateau (China). Quat. Sci. Rev. 39, 73–85. https://doi.org/10.1016/j.quascirev.2012.02.011.
Kasper, T., Wang, J., Schwalb, A., Daut, G., Plessen, B., Zhu, L., Mäusbacher, R., Haberzettl, T., 2021. Precipitation dynamics on the Tibetan Plateau during the Late Quaternary - hydroclimatic sedimentary proxies versus lake level variability. Global Planet. Change 205, 103594. https://doi.org/10.1016/j.gloplacha.2021.103594.
Kastner, S., Ohlendorf, C., Haberzettl, T., Lücke, A., Mayr, C., Maidana, N.I., Schäbitz, F., Zolitschka, B., 2010. Southern hemispheric westerlies control the spatial distribution of modern sediments in Laguna Potrok Aike, Argentina. J. Paleolimnol. 44 (4), 887–902. https://doi.org/10.1007/s10933-010-9462-0.
Kazakov, M., 1929. Hydrological researches in the western-shore region of Lake Gokcha. In: Loewinson-Lessing, F. (Ed.), Le Bassin du lac Sevan (Goktcha): Résultats scientifiques de l'expédition de 1927/Bassejn ozera Sevan (Gokča), pp. 515–516. Leningrad.
Kirschvink, J.L., 1980. The least-squares line and plane and the analysis of palaeomagnetic data. Geophys. J. Roy. Astron. Soc. 62 (3), 699–718. https://doi.org/10.1111/j.1365-246X.1980.tb02601.x.
Legovich, N.A., Markosian, A.G., Meshkova, T.M., A.I, S., 1973. Physico-chemical regime and bioproductive processes in Lake Sevan (Armenia) in transition from oligotrophy to eutrophy. SIL Proceedings 18, 1835–1842.
Leroyer, C., Joannin, S., Aoustin, D., Ali, A.A., Peyron, O., Ollivier, V., Tozalakyan, P., Karakhanyan, A., Jude, F., 2016. Mid Holocene vegetation reconstruction from Vanevan peat (south-eastern shore of Lake Sevan, Armenia). Quat. Int. 395, 5–18. https://doi.org/10.1016/j.quaint.2015.06.008.
Loewinson-Lessing, F., 1929. On utilizing lake gokcha (sevan) for irrigation. In: Loewinson-Lessing, F. (Ed.), Le Bassin du lac Sevan (Goktcha): Résultats scientifiques de l'expédition de 1927/Bassejn ozera Sevan (Gokča), pp. 527–529. Leningrad.
Meyers, S., 2014. Astrochron: an R Package for Astrochronology.
Mischke, S., 2020. Preface. In: Mischke, S. (Ed.), Large Asian Lakes in a Changing World. Springer, Cham. v-vii.
Niemann, H., Haberzettl, T., Behling, H., 2009. Holocene climate variability and vegetation dynamics inferred from the (11700 cal. yr BP) Laguna Rabadilla de Vaca sediment record, southeastern Ecuadorian Andes. Holocene 19 (2), 307–316. https://doi.org/10.1177/0959683608100575.
Ohlendorf, C., Gebhardt, C., Hahn, A., Kliem, P., Zolitschka, B., 2011. The PASADO core processing strategy — a proposed new protocol for sediment core treatment in multidisciplinary lake drilling projects. Sediment. Geol. 239 (1), 104–115. https://doi.org/10.1016/j.sedgeo.2011.06.007.
Peck, J.A., King, J.W., Colman, S.M., Kravchinsky, V.A., 1996. An 84-kyr paleomagnetic record from the sediments of Lake Baikal, Siberia. J. Geophys. Res. 101 (B5), 11365–11385. https://doi.org/10.1029/96JB00328.
R Core Team, 2024. R: A Language and Environment for Statistical Computing.
Reimer, P.J., Austin, W.E.N., Bard, E., Bayliss, A., Blackwell, P.G., Bronk Ramsey, C., Butzin, M., Cheng, H., Edwards, R.L., Friedrich, M., Grootes, P.M., Guilderson, T.P., Hajdas, I., Heaton, T.J., Hogg, A.G., Hughen, K.A., Kromer, B., Manning, S.W., Muscheler, R., Palmer, J.G., Pearson, C., van der Plicht, J., Reimer, R.W., Richards, D.A., Scott, E.M., Southon, J.R., Turney, C.S.M., Wacker, L., Adolphi, F., Büntgen, U., Capano, M., Fahrni, S.M., Fogtmann-Schulz, A., Friedrich, R., Köhler, P., Kudsk, S., Miyake, F., Olsen, J., Reinig, F., Sakamoto, M., Sookdeo, A., Talamo, S., 2020. The IntCal20 northern hemisphere radiocarbon age calibration curve (0–55 cal kBP). Radiocarbon 62 (4), 725–757. https://doi.org/10.1017/RDC.2020.41.
Rivero-Montero, M., Gómez-Paccard, M., Kondopoulou, D., Tema, E., Pavón-Carrasco, F. J., Aidona, E., Campuzano, S.A., Molina-Cardín, A., Osete, M.L., Palencia-Ortas, A., Martín-Hernández, F., Rubat-Borel, F., Venturino, M., 2021. Geomagnetic field intensity changes in the central mediterranean between 1500 BCE and 150 CE: Implications for the levantine iron age anomaly evolution. Earth Planet Sci. Lett. 557, 116732 https://doi.org/10.1016/j.epsl.2020.116732.
Robles, M., Peyron, O., Brugiapaglia, E., Menot, G., Dugerdil, L., Ollivier, V., Ansanay-Alex, S., Develle, A.L., Tozalakyan, P., Meliksetian, K., Sahakyan, K., Sahakyan, L., Perello, B., Badalyan, R., Colombie, C., Joannin, S., 2022. Impact of climate changes on vegetation and human societies during the Holocene in the South Caucasus (Vanevan, Armenia): a multiproxy approach including pollen, NPPs and brGDGTs. Quat. Sci. Rev. 277, 107297 https://doi.org/10.1016/j.quascirev.2021.107297.
Sarkisyan, S.G., 1962. Petro-mineralogical Studies of the Lake Sevan Basin. Publishing house of the Academy of Sciences of Armenia. SSR, Yerevan.
Satian, M.A., Chilingaryan, G.V., 1994. Geology of Sevan. Yerevan, National Academy of Sciences of the Republic of Armenia.
Satian, M.A., Stepanyan, Z.O., Zhamgorcyan, V.N., 1968. Otkrytie vulkanicheskih shlakov i peplov sredi donnyh osadkov oz. Sevan (Discovery of volcanic scoria and ashes among the bottom sediments of the Sevan Lake). Proceedings of AS of Arm SSR, Earth Sciences 3, 62–71.
Sayadyan, Y.V., 2000 (in Russian). Fluctuations of the Shoreline of Lake Sevan in the Holocene (Armenia), vol. 132. St. Petersburg News Russian Geogr. Soc. Publishing house Nauka, pp. 37–47, 3.
Sayadyan, Y.V., Aleshinskaya, Z.V., Ryabova, E.I., 1974. Holocene sediments of the western shore of Lake Sevan. Proc. Acad. Sci. Arm SSR Earth Sci. 27 (6), 3–10.
Scafetta, N., Milani, F., Bianchini, A., Ortolani, S., 2016. On the astronomical origin of the Hallstatt oscillation found in radiocarbon and climate records throughout the Holocene. Earth Sci. Rev. 162, 24–43. https://doi.org/10.1016/j.earscirev.2016.09.004.
Sherriff, J.E., Wilkinson, K.N., Adler, D.S., Arakelyan, D., Beverly, E.J., Blockley, S.P.E., Gasparyan, B., Mark, D.F., Meliksetian, K., Nahapetyan, S., Preece, K.J., Timms, R.G. O., 2019. Pleistocene volcanism and the geomorphological record of the Hrazdan valley, central Armenia: linking landscape dynamics and the Palaeolithic record. Quat. Sci. Rev. 226, 105994 https://doi.org/10.1016/j.quascirev.2019.105994.
Shikhani, M., Mi, C., Gevorgyan, A., Gevorgyan, G., Misakyan, A., Azizyan, L., Barfus, K., Schulze, M., Shatwell, T., Rinke, K., 2021. Simulating thermal dynamics of the largest lake in the Caucasus region: the mountain Lake Sevan. J. Limnol. 81 (s1) https://doi.org/10.4081/jlimnol.2021.2024.
Sigg, L., Stumm, W., 1996. Aquatische Chemie. Teubner, Stuttgart.
Steinhilber, F., Abreu, J.A., Beer, J., Brunner, I., Christl, M., Fischer, H., Heikkilä, U., Kubik, P.W., Mann, M., McCracken, K.G., Miller, H., Miyahara, H., Oerter, H., Wilhelms, F., 2012. 9,400 years of cosmic radiation and solar activity from ice cores and tree rings. In: Proceedings of the National Academy of Sciences of the United States of America, 109, pp. 5967–5971. https://doi.org/10.1073/pnas.1118965109 (16).
Stoner, J.S., St-Onge, G., 2007. Magnetic stratigraphy in paleoceanography: Reversals, excursions, paleointensity and secular variation. In: Hillaire-Marcel, C., de Vernal, A. (Eds.), Proxies in Late-Cenozoic Paleoceanography. Elsevier, pp. 99–138.
Stuiver, M., Reimer, P.J., Reimer, R.W., 2020. Calib 8.2. Radiocarbon 35, 215–230 [WWW program].
Taner, M.T., 1992. Attributes revisted. Technical Report. Rock Solid Images. Inc.
Turtsev, A., 1929. A hydrogeological sketch of the north-western shores of Lake Gokcha. In: Loewinson-Lessing, F. (Ed.), Le Bassin du lac Sevan (Goktcha): Résultats scientifiques de l'expédition de 1927/Bassejn ozera Sevan (Gokča), pp. 519–520. Leningrad.
Ulyanova, D.S., 1993. The precipitation of $CaCO_3$: a mechanism of self regulation of the Lake Sevan ecosystem. Hydrological,. Chemical and Biological Processes of Transformation and Transport of Contaminants in Aquatic Environments. lAHS, Rostov-on-Don Symposium.
Usoskin, I.G., 2023. A history of solar activity over millennia. Living Rev. Sol. Phys. 20 (1), 2. https://doi.org/10.1007/s41116-023-00036-z.
Usoskin, I.G., Gallet, Y., Lopes, F., Kovaltsov, G.A., Hulot, G., 2016. Solar activity during the Holocene: the Hallstatt cycle and its consequence for grand minima and maxima. Astronomy & Astropysics 587, A150. https://doi.org/10.1051/0004-6361/201527295.
Vardanyan, A.A., Korzhenkov, A.M., Sorokin, A.A., Stakhovskaya, R.Y., 2018. Paleogeographic conditions and age of a strong Earthquake according to data from studying of the Holocene Deposits from Lake Sevan, Armenia. Izvestiya Atmos. Ocean. Phys. 54 (8), 859–866. https://doi.org/10.1134/S0001433818080145.
Wilkinson, I.P., 2020. Lake Sevan: Evolution, biotic variability and ecological degradation. In: Mischke, S. (Ed.), Large Asian Lakes in a Changing World: Natural State and Human Impact. Springer International Publishing, Cham, pp. 35–63. https://doi.org/10.1007/978-3-030-42254-7_2.
Wilkinson, I.P., Gulakyan, S.Z., 2010. Holocene to recent Ostracoda of Lake Sevan, Armenia: Biodiversity and ecological controls. Stratigraphy 7 (4), 301–315.
Wilkinson, I.P., Bubikyan, S.A., Gulakyan, S.Z., 2005. The impact of late Holocene environmental change on lacustrine Ostracoda in Armenia. Palaeogeogr. Palaeoclimatol. Palaeoecol. 225 (1), 187–202. https://doi.org/10.1016/j.palaeo.2005.06.010.
Zavalishin, A., 1929. Investigations of the soil covering of the northern shore of Lake Gokcha. In: Loewinson-Lessing, F. (Ed.), Le Bassin du lac Sevan (Goktcha): Résultats scientifiques de l'expédition de 1927/Bassejn ozera Sevan (Gokča), pp. 521–522. Leningrad.